

TRATSS: Transformer-Based Task Scheduling System for Autonomous Vehicles

Yazan Youssef, *Member, IEEE*, Paulo Ricardo Marques de Araujo, *Member, IEEE*, Aboelmagd Noureldin, *Senior Member, IEEE*, and Sidney Givigi, *Senior Member, IEEE*

Abstract—Efficient scheduling remains a critical challenge in various domains, requiring solutions to complex NP-hard optimization problems to achieve optimal resource allocation and maximize productivity. In this paper, we introduce a framework called Transformer-Based Task Scheduling System (TRATSS), designed to address the intricacies of single agent scheduling in graph-based environments. By integrating the latest advancements in reinforcement learning and transformer architecture, TRATSS provides a novel system that outputs optimized task scheduling decisions while dynamically adapting to evolving task requirements and resource availability. Leveraging the self-attention mechanism in transformers, TRATSS effectively captures complex task dependencies, thereby providing solutions with enhanced resource utilization and task completion efficiency. Experimental evaluations on benchmark datasets demonstrate TRATSS’s effectiveness in providing high-quality solutions to scheduling problems that involve multiple action profiles.

Index Terms—Scheduling, reinforcement learning, optimization, graph neural networks, transformers.

I. INTRODUCTION

Efficient allocation of resources to tasks is a critical challenge in domains such as logistics, industrial production, and project management [1].

Traditional approaches often involve complex combinatorial optimization, requiring sophisticated algorithms to navigate the wide range of possible task combinations for optimal decision-making [2].

Over the past decade, scheduling has advanced significantly, particularly using greedy algorithms and heuristics [3]. However, these methods often struggle to scale efficiently in complex real-world scenarios and require considerable time to produce solutions [2].

In response to these challenges, researchers have turned their attention to advanced optimization techniques like integer linear programming (ILP) [4], constraint programming (CP) [5], and meta-heuristic algorithms such as genetic algorithms [6], and simulated annealing [7]. These methods, applied to problems like the Traveling Salesperson Problem (TSP), have shown promise but often struggle with scalability

and finding optimal solutions in complex, large-scale scheduling problems [8]. These limitations have led to the adoption of machine learning approaches, particularly reinforcement learning (RL), which uses actions within an environment to achieve efficient scheduling [8].

Meanwhile, the emergence of transformer architecture has revolutionized fields like natural language processing (NLP) and sequential data processing [9], [10]. Originally developed for machine translation [11], transformers are now the foundation of state-of-the-art NLP models like BERT and GPT [10]. Their use of self-attention mechanisms to capture long-range dependencies in sequences makes them highly effective for capturing complex patterns and relationships in data, making them well-suited for sequential decision-making tasks such as scheduling [12].

Inspired by the success of transformers in NLP, researchers are now exploring their use in combinatorial optimization problems like task assignment and scheduling [13]. Transformers’ ability to model complex task-resource relationships, along with their scalability and parallelizability, make them a promising tool for enhancing task allocation, particularly when combined with RL [14]. This paper aims to investigate the application of transformers and RL in constraint-based scheduling problems.

The main contribution of this paper is TRATSS, a scheduling system that leverages transformers for scheduling multi-stage tasks on graph-based problems for a single agent. To the best of our knowledge, this framework is the first of its kind. TRATSS is shown to provide good solutions, in seconds, regardless of the problem configuration. For the sake of demonstration, TRATSS was used in a search and rescue mission, showcasing its ability to schedule an Unmanned Aerial Vehicle (UAV) to search a series of locations of varying sizes as well as its generalization capabilities.

The paper is organized as follows. Section II reviews machine learning approaches for scheduling and path planning, while identifying gaps on a systematic approach for the application of such approaches. Section III presents the scheduling problem mathematically. Section IV details TRATSS. Section V describes the simulation setup and the tested scenarios. Section VI presents the simulation results; and Section VII concludes the paper.

II. RELATED WORK

There has been limited work on multi-stage graph-based scheduling and planning using machine learning, as innovations in this area, particularly with graph neural networks

Y. Youssef is with the Department of Electrical and Computer Engineering, Queen’s University, Kingston, ON, Canada (e-mail: yazan.youssef@queensu.ca).

A. Noureldin is with the Department of Electrical and Computer Engineering at the Royal Military College of Canada, and the Department of Electrical and Computer Engineering at Queen’s University, both in Kingston, Canada (e-mail: aboelmagd.noureldin@rmc.ca).

S. Givigi and P. Araujo are with the School of Computing, Queen’s University, Kingston, ON, Canada (e-mail: {sidney.givigi, paulo.araujo}@queensu.ca).

(GNNs), are relatively recent [15]. The most closely related work is by Joshi et al. in [16]. Li et al. [17] also contribute by processing large-scale graphs with GNNs, integrating a key-query mechanism for encoding, and using a multi-layer perceptron (MLP) for decoding. Another related study proposes a recursive graph grammar for optimizing UAV formations to efficiently complete missions [18].

Other works focus on task assignment planning using methods like recursive recurrent networks (RNN) with particle swarm optimization (PSO) [19] or deep reinforcement learning (DRL) [20]. Beyond general planning, research is also advancing in specific areas like task assignment and motion planning (TAMP) in the context of robotics [21]. For example, Wang et al. [22] use the A^* algorithm for high-level path planning and RL for motion planning. Recent studies aim to integrate task assignment and path planning for simultaneous optimization, which is expected to yield better results [23].

In addition to previous research, other studies focus on task assignment, scheduling, and planning for multi-vehicle missions and applications. Niu et al. [12] uses a deep Q-learning network (DQN) to resemble a control center for UAV task scheduling in a disaster scenario. Bai et al. [24] address capacity-constrained heterogeneous delivery problems with a heuristic algorithm. Chen et al. [23] develop a framework for task assignment and path planning in pick-up-delivery contexts. Li et al. [14] use an RL-trained network to handle task assignment in warehouse order collection, framing it as a multiple depot TSP (MDTSP). Yin et al. [25] explore high-level task assignment for crowd-sensing. Huang et al. [26] use deep RL to perform joint optimization of computation offloading and resource allocation in internet of vehicles. Huang et al. [27] propose an RL approach to optimize vehicle scheduling in car-hailing platforms.

There is a notable lack of systems-level analysis in the literature on applying machine learning to scheduling, particularly to graph-based scheduling. One of the few papers addressing the use of RL for systematic scheduling is [28]. However, its focus is on job shop scheduling rather than scheduling for moving agents.

In contrast, this paper proposes a novel framework that fully solves multi-stage scheduling using deep learning and can be adapted for various applications involving vehicles or mobile robots. While a search and rescue scenario was tested, the framework is general and applicable to other robotic scenarios. As shown in Section VI, it can solve the traditional TSP and easily extend to the Traveling Repairman Problem (TRP) [29], [30], where tasks vary in duration. Hence, it can be utilized in several types of missions, from surveillance to agricultural tasks.

III. PROBLEM FORMULATION

The problem we solve with TRATSS can be formulated similarly to the TRP. Given a graph $G = (V, E)$, $V = \{1, 2, \dots, n\}$ is a set of areas to be visited, where $\{0\}$ is the arbitrary initial point of the path, and $E = \{(i, j) : i, j \in V, i \neq j\}$ is the connections between areas. The objective is for the agent to visit all the areas once with the shortest path.

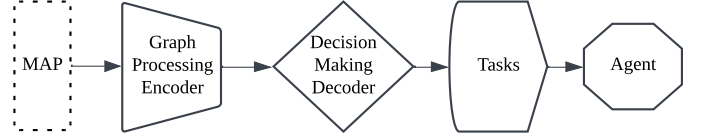


Fig. 1: System workflow.

Note that here we use “shortest path” in a loose sense, as this does not refer necessarily to distance, but to a cost, which can be time, energy, or another metric. For simplicity and compliance to the literature, from now on we use “distance” to mean “cost”.

Since the areas are not dimensionless, i.e., we are not dealing with only points, the distance d_{ij} between two different areas i and j , with $(i, j) \in E$ can be different depending on the starting and end points chosen by the agent. Therefore, the distance is defined as $d_{ij} = \|s_j - e_i\|$, i.e., the Euclidean distance between the selected starting point in area j and the endpoint in area i .

The selection of start and end points for the trajectory is crucial for minimizing distance. The area can have any shape and the agent can enter or leave the area anywhere depending on the chosen or predefined movement pattern for that area. A scenario might consist of multiple areas with different properties requiring specific scanning methods. For example, dense tree canopies may need a compact zig-zag pattern to maximize coverage, whereas open areas could benefit from sparser movement patterns like spirals or stars. Another scenario involves the flexibility to select any movement pattern for any area, and this is the focus of this work.

Therefore, given G and any set of possible movement patterns, the scheduling system must determine the shortest path such that the agent (1) visits each area exactly once, (2) starts and ends at the same area, and (3) accounts for the movement pattern chosen for each area.

IV. TRATSS

TRATSS addresses a single-agent scheduling problem with multiple decisions, as described in Section III. Using a map of the region of interest as input, TRATSS employs artificial neural networks to generate an optimized task sequence, minimizing execution costs, such as distance and time. This approach is similar to the TRP, where minimizing distance is equivalent to minimizing time if the agent travels at a constant speed, with the pattern selection affecting the service time for each area. The pattern selection determines the landing point of the agent, which in turn affects the distance and time that the agent needs to reach the next area.

Based on Joshi et al.’s pipeline [16], TRATSS adapts key components to meet the specific objectives of this problem. The system overview is illustrated in Fig. 1, with its components detailed in the following sections.

A. Input Map

A map indicating the areas that need to be scanned is inputted into the system. Geometric approximations for the

areas (e.g., rectangular shapes) are used to build the input map, capturing and describing the locations and features of the areas that must be visited. Each input map is composed of 3 matrices: adjacency matrix $A \in \mathbb{R}^{n \times n}$, feature matrix $X \in \mathbb{R}^{n \times f}$, and a position matrix $P \in \mathbb{R}^{n \times 2}$, where n and f are the number of areas and the number of features, respectively. For example, in the demonstration scenario detailed in section V-A, the areas were defined by rectangular frames using 4 corners determining their borders. Therefore, f was set to 8, corresponding to four pairs of (x, y) coordinates, as shown in Fig. 2a.

The adjacency matrix A describes the connectivity of the areas, and the feature matrix X contains the features used for describing the areas. The feature matrix is used to calculate d_{ij} . Finally, the position matrix P contains the centers of the areas in the map, which are the same as the centers of the frames.

B. Encoder

The encoder, in Fig. 2b, transforms the input map into a d_1 -dimensional representation using a graph neural network (GNN). Specifically, it converts the feature matrix $X \in \mathbb{R}^{n \times f}$ into $X_1 \in \mathbb{R}^{n \times d_1}$ with a Gated Graph ConvNet [31]. This GNN, comprising L layers, uses anisotropic aggregation and a gating mechanism to refine node and edge features through recursive message passing, improving graph representation. Hence, the node feature h_i^ℓ and edge feature e_{ij}^ℓ at layer ℓ are:

$$h_i^{\ell+1} = h_i^\ell + \text{ReLU} \left(\text{BN} \left(U^\ell h_i^\ell + \text{AG}_{j \in \mathcal{N}_i} \left(\sigma(e_{ij}^\ell) \odot V^\ell h_j^\ell \right) \right) \right), \quad (1)$$

$$e_{ij}^{\ell+1} = e_{ij}^\ell + \text{ReLU} \left(\text{BN} \left(A^\ell e_{ij}^\ell + B^\ell h_i^\ell + C^\ell h_j^\ell \right) \right), \quad (2)$$

where $U^\ell, V^\ell, A^\ell, B^\ell, C^\ell \in \mathbb{R}^{d_1 \times d_1}$ are the learnable parameters of the encoder, ReLU represents the Rectified Linear Unit function, BN represents the batch normalization layer, AG is the neighborhood aggregation function, σ is the sigmoid function, and \odot is the Hadamard product. For the first layer ($\ell = 0$), the inputs h_i^0 and e_{ij}^0 are d_1 -dimensional linear projections of the feature matrix X and the Euclidean distance between the centers of the areas $\|p_i - p_j\|$, respectively.

C. Decoder

The decision decoder, illustrated in Fig. 1, employs an autoregressive transformer architecture for decoding and decision-making. Transformers are effective for handling long sequences with dependencies [10]. Therefore, the proposed decoder consists of three sequential attention networks (illustrated in Fig. 2c):

- 1) **Network I** selects the next area to visit.
- 2) **Network II** determines the starting point in the area.
- 3) **Network III** decides the movement pattern for the area.

Each one of these networks follows the sequence: Input Embedding, Multi-Head Attention, Embedding, Attention, and Softmax.

Network [I], which chooses the next area, uses the encoder's output to build an initial context representation \hat{h}_i^C for the current node i at time step t . This context, given by

$$\hat{h}_i^C = W_F \left[h_G, h_{\pi'_1}^L, h_{\pi'_{t-1}}^L \right], \quad h_G = \frac{1}{n} \sum_{i=0}^n h_i^L, \quad (3)$$

includes learnable weights $W_F \in \mathbb{R}^{d_1 \times d_1}$ and averages the features from the encoder. Here, $h_{\pi'_1}^L$ and $h_{\pi'_{t-1}}^L$ are features of the first and last areas in the partial tour (π') up to $t-1$. This context \hat{h}_i^C is used to highlight the correlation between the current area and the existing tour, as illustrated in the first component of Fig. 2c.

The initial context (3) is refined using Multi-Head Attention (MHA) over the node embeddings. We define the parameters of the first MHA (MHA₁) as $Q_1 = W_{C_1} \hat{h}_i^C$, $K_1 = \{W_{A_1}[h_1^L, \dots, h_n^L]\}$, and $V_1 = \{W_{A_2}[h_1^L, \dots, h_n^L]\}$, where $W_{C_1}, W_{A_1}, W_{A_2} \in \mathbb{R}^{d_1 \times d_1}$ are learnable parameters. Q_1 represents our current knowledge, while K_1 and V_1 represent the options for the output. The MHA operation is then given by:

$$h_i^C = \text{MHA}_1(Q_1, K_1, V_1). \quad (4)$$

The unnormalized logit for choosing the next area j (or edge e_{ij}) is computed using an attention mechanism between the context h_i^C from (4) and the embedding h_j^L :

$$\hat{p}[A_j|A_i] = M \cdot \tanh \left(\frac{(W_{Q_1} h_i^C)^T \cdot (W_{K_1} h_j^L)}{\sqrt{d_1}} \right), \quad (5)$$

where $j \neq \pi'_t$. If j is already part of the tour, $\hat{p}[A_j|A_i] = \infty$. $W_{Q_1}, W_{K_1} \in \mathbb{R}^{d_1 \times d_1}$ are learnable parameters, and \tanh keeps the logits in the range $[-M, M]$. The logits are then converted to probabilities $p[A_j|A_i]$ via a softmax operation.

This formulation, based on [16], addresses traditional TSPs. The following sections extend this to enable TRATSS to perform task assignments and solve TRPs.

After selecting area j using (5), the features of area j are used to determine the starting point. As illustrated in the middle component of Fig. 2c, the (x, y) coordinates of the features of area j and the current location coordinates are fed into the Network [II]. The current location is where the agent ended up in area i at step $t-1$.

A context representation for the current location is created using MHA over the corner coordinates of area j . This context is used to correlate the agent's location to the possible starting locations in the chosen area. The coordinates of the current location and the features are embedded using a feedforward linear network, resulting in d_2 -dimensional embeddings:

$$h_{st} = W_{C_2} h_{\text{current}}, \quad W_\Lambda[h_1, h_2, h_3, h_4]$$

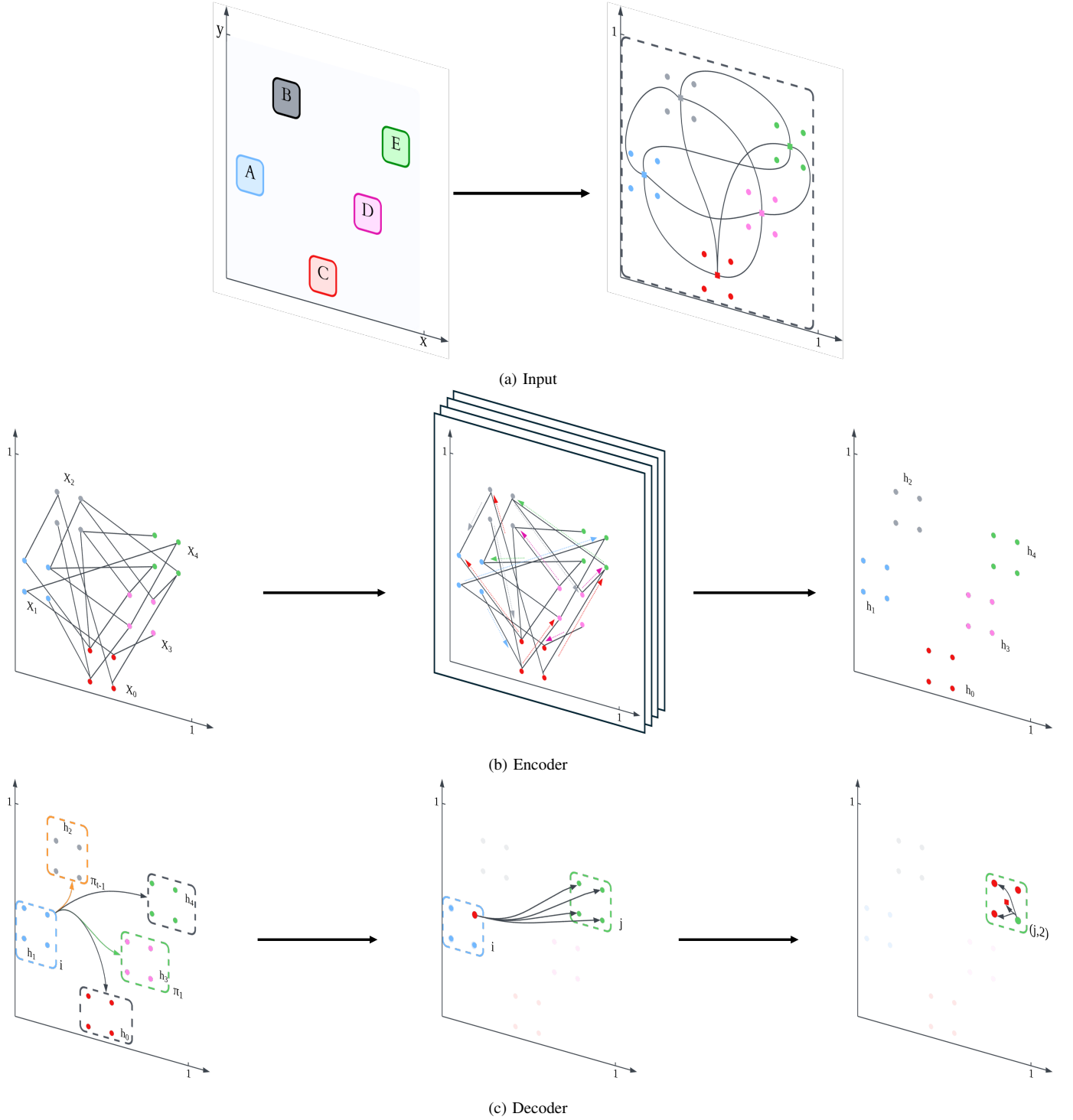


Fig. 2: TRATSS. (a) The map is normalized and the required features are extracted, (b) The encoder then processes the input features through GNN to obtain a new feature representation, and (c) The decoder processes the new features in 3 networks: the first network selects the next area to visit, the second network assigns the starting point in the chosen area, and finally the third network decides the movement pattern to be followed.

where $h_{current} = (x_{current}, y_{current})$, $[h_1, h_2, h_3, h_4]$ are the corner coordinates, and $W_{C_2}, W_{\Lambda} \in \mathbb{R}^{d_2 \times 2}$ are trainable parameters. MHA₂ parameters are:

$$\begin{aligned} Q_2 &= h_{st}, \\ K_2 &= \{W_{\Lambda 1}[h_1, h_2, h_3, h_4]\}, \\ V_2 &= \{W_{\Lambda 2}[h_1, h_2, h_3, h_4]\}. \end{aligned}$$

The MHA operation yields the context h_{st}^C :

$$h_{st}^C = \text{MHA}_2(Q_2, K_2, V_2). \quad (6)$$

The unnormalized logit for choosing corner h_k , $k \in \{1, 2, 3, 4\}$, as the starting point is calculated using an attention mechanism between h_{st}^C and h_k :

$$\hat{p}[\Lambda_k | A_j] = M \cdot \tanh \left(\frac{(W_{Q_2} h_{st}^C)^T \cdot (W_{K_2} h_k)}{\sqrt{d_2}} \right), \quad (7)$$

Finally, the logits $\hat{p}[\Lambda_k | A_j]$ are converted to probabilities $p[\Lambda_k | A_j]$ using a softmax operation.

The final step of the decoder is to choose the pattern the agent should follow. This is done similarly to the previous steps. The coordinates of the stopping points for each pattern (h_{P_z}) along with the starting point h_k obtained from Network [II], are fed into Network [III], as illustrated in the third component of Fig. 2c.

First, a context representation for point h_k is created using MHA over the possible stopping points associated with the patterns. Assuming there are p possible patterns, the coordinates of h_k and the stopping points from patterns P_1, P_2, \dots, P_p are embedded using a d_3 -dimensional input embedding layer. MHA₃ parameters are:

$$\begin{aligned} Q_3 &= W_{C_3}[h_k], \\ K_3 &= \{W_{\Psi_1}[h_{P_1}, h_{P_2}, \dots, h_{P_p}]\}, \\ V_3 &= \{W_{\Psi_2}[h_{P_1}, h_{P_2}, \dots, h_{P_p}]\} \end{aligned}$$

where $W_{C_3}, W_{\Psi_1}, W_{\Psi_2} \in \mathbb{R}^{d_3 \times 2}$ are the trainable weight matrices. The context representation for selecting the pattern is then:

$$h_k^C = \text{MHA}_3(Q_3, K_3, V_3). \quad (8)$$

The unnormalized logit for selecting pattern P_z , $z \in \{1, 2, \dots, p\}$, is computed using a final attention mechanism between the context h_k^C (from (8)) and the coordinates of the stopping point from pattern P_z (h_{P_z}):

$$\hat{p}[\Psi_z | A_j, \Lambda_k] = M \cdot \tanh \left(\frac{(W_{Q_3} h_k^C)^T \cdot (W_{K_3} h_{P_z})}{\sqrt{d_3}} \right), \quad (9)$$

where $W_{Q_3} \in \mathbb{R}^{d_3 \times d_3}$ and $W_{K_3} \in \mathbb{R}^{d_3 \times 2}$ are learnable parameters. The logits $\hat{p}[\Psi_z | A_j, \Lambda_k]$ are converted to probabilities using softmax over all patterns. A pattern Ψ_z is selected, and its associated stopping point becomes the current location for the next step. The final probability of the action (choosing area A_j , starting point h_k , and pattern P_z) is:

$$p[j, k, z] = p[A_j] \cdot p[\Lambda_k | A_j] \cdot p[\Psi_z | A_j, \Lambda_k]. \quad (10)$$

This process repeats until all areas are covered. Consequently, the final output of the decoder is the sequence of tasks that will be followed by the agent.

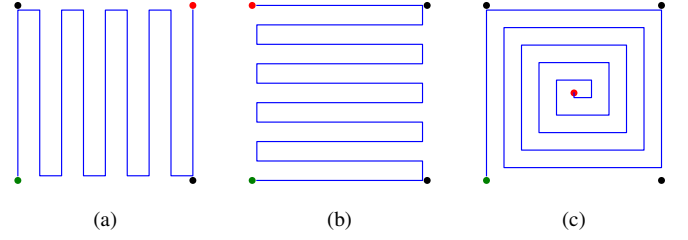


Fig. 3: Available patterns. (a) Vertical Zig-Zag, (b) Horizontal Zig-Zag, and (c) Spiral.

D. RL Policy Training

RL is highly effective for training networks in scenarios where ground truth solutions are unavailable, as in the case of search and rescue task scheduling. In this paper, we use the REINFORCE policy gradient algorithm due to its simplicity. The objective is to minimize the total distance covered in a given scenario, which in turn would minimize the total execution time of the mission. The loss for an instance s parameterized by θ is defined as $\mathcal{L}(\theta|s) = \mathbb{E}_{p_\theta(\pi|s)}[L(\pi)]$, where $L(\pi)$ is the tour length and $p_\theta(\pi|s)$ is the probability distribution of the tour π .

The gradient for minimizing \mathcal{L} using REINFORCE is:

$$\nabla \mathcal{L}(\theta|s) = \mathbb{E}_{p_\theta(\pi|s)}[(L(\pi) - b(s)) \nabla \log(p_\theta(\pi|s))], \quad (11)$$

where $b(s)$ is a baseline to reduce gradient variance. Here, $L(\pi)$ is the tour length per epoch, and $p_\theta(\pi|s)$ is the probability of the tour, calculated as the product of action probabilities $p[j, k, z]$ from (10).

V. SIMULATION SETUP

A. Scenario

To demonstrate TRATSS's effectiveness, we tested the proposed system in a scenario that can illustrate a search-and-rescue application, where an agent has to visit several areas in the shortest distance/time possible. Without loss of generality, we represent the areas as squares, where they are defined by their four corners, resulting in a feature matrix $X \in \mathbb{R}^{n \times 8}$, corresponding to four pairs of (x, y) coordinates.

Additionally, we define three possible movement patterns for the agent: Vertical lawn mower, horizontal lawn mower, or spiral, as shown in Fig. 3, where the green and red dots represent the starting and ending positions, respectively.

B. Dataset

For training, n areas, represented by frames, were generated within a unit square. Each area center was sampled from a uniform distribution $C = (c_x, c_y)$ where $c_x, c_y \in [0, 1]$. Then a random radius $r \in [0.01, 0.03]$ was added and subtracted from the center coordinates to form the four corners. This process was repeated until all n areas were generated, ensuring they stayed within the unit square and did not overlap. The unit square was chosen for easy scalability. In total, the dataset comprises 128,000 randomly generated maps.

C. Hyper-parameters

For the encoder, 3 layers were used, with hidden dimension $d_1 = 128$. Following the encoder, the decoder consists of the 3 parts as discussed in Section IV-C. For $P[A_j|A_i]$ given in (5), we used $d_1 = 128$ for the hidden dimension and 8 heads for the MHA network. For $P[\Lambda_k|A_j]$ and $P[\Psi_z|A_j, \Lambda_k]$ given in (7) and (9), respectively, we used $d_2 = d_3 = 128$ for the hidden dimension and a single head for their respective MHA networks. The described configuration resulted in approximately 360,000 trainable parameters.

D. Training Process

The training was conducted for 100 epochs, with each epoch generating 128,000 maps, divided into 1,000 batches of 128. The model was trained using the Adam optimizer with a fixed learning rate of 10^{-4} . The RL environment was developed using GYM [32], chosen for its compatibility with the Robot Operating System (ROS) [33], [34], facilitating easy future deployment on real robots. The proposed model was implemented using PyTorch 2.1, an NVIDIA GeForce 3090, and an Intel i9 11900KF Eight-Core Processor 3.5GHz (5.3GHz With Turbo Boost).

E. Evaluation Metrics and Compared Methods

To evaluate the performance of the proposed method, the following tests were conducted:

- 1) **TSP Validation:** The environment's behavior was verified using the dataset from [16], comparing results against the baseline. This test was used to verify the functionality of Network I.
- 2) **Decoder Functionality:** Separate tests were conducted for the start/end points and pattern elements using two evaluation sets with 1,280 map samples of 15 and 20 areas. The entry and exit points were fixed for all the areas in the evaluation set. An edge weight matrix was then provided accordingly to Concorde solver and its results were used as a baseline. Network III was disabled, by fixing the pattern, to verify the functionality of Network II when connected to Network I.
- 3) **System Assessment:** The full system was finally tested against Concorde solver results. For this test, TRATSS was expected to outperform Concorde by considering the cost of selecting new start/end points for patterns.
- 4) **Scaling capabilities:** A final test with 30, 40 and 50 areas were conducted to evaluate the performance of the proposed model in previously unseen environments, i.e., more areas than the number of areas used to train the model.

The evaluation metric used, known as the optimality gap, $o_g \in \mathbb{R}$, follows the standard approach in the literature [16] and is defined as

$$o_g = \left(\frac{l_m}{l_s} \right) \cdot 100, \quad (12)$$

where $l_m, l_s \in \mathbb{R}$ are the model and solver tour lengths, respectively.

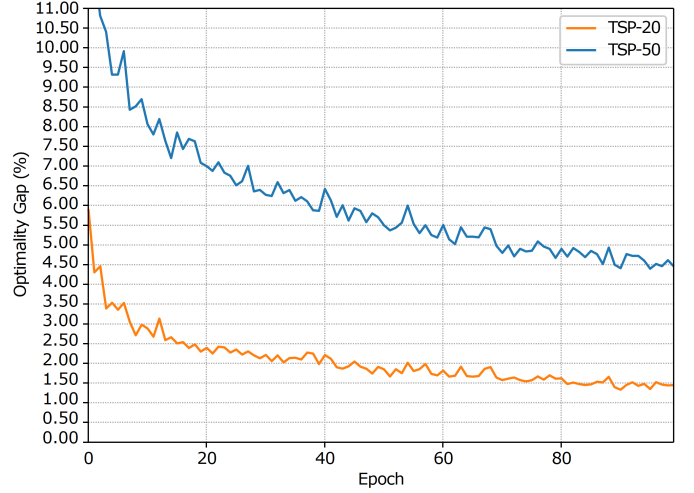


Fig. 4: Pure TSP results.

The solver used in these tests is the Concorde solver [35]. Concorde's TSP solver is an LP-based program designed to solve TSP-like problems. It has been used to obtain the optimal solutions to the full set of 110 TSPLIB instances. Hence, its solution was used as the ground truth solution when evaluating TRATSS's performance, as it is known to provide *optimal* solutions to TSP and TSP-like problems.

For the baseline in (11), we used a greedy rollout approach [36]. The model in step t of the training is frozen and serves as the baseline updated every $u = 1000$ steps. Each epoch consists of 1000 steps, with the baseline updated at the end of each epoch. For real scenario testing (as discussed in item 4 above), we used a critic baseline [8] for comparison. In the critic baseline, $b(s)$ in (11) is defined as $b(s) = \hat{v}(s, \mathbf{w})$, where $\hat{v}(s, \mathbf{w})$ is a learned value function parameterized by \mathbf{w} . The critic network consists of a linear feedforward layer, the encoder IV-B, and two consecutive linear feedforward layers.

VI. RESULTS

A. TSP Validation

The results from the first test, shown in Fig. 4, align with those reported by Joshi et al. [16] [Figure 11, TSP-50, $L=3$, $d=128$ (RL)]. The 100 epochs in Fig. 4 represent 12.8 million samples in their study. This confirms that our environment can replicate the results of [16]. Although we used fewer samples, the goal was to validate that the framework, with the two MHA operations described in (6) and (8), performs as expected.

B. Decoder Functionality

After confirming the system could solve the TSP, we conducted a second test. Here, starting and stopping points in each area were fixed, and the problem was treated as a pure TSP by the Concorde solver. The challenge here was in defining the edge matrix E , explained in Section III. Concorde can only provide solutions when the provided E is symmetric with integer elements. However, E in this test was not symmetric and the its elements were all float numbers due to map

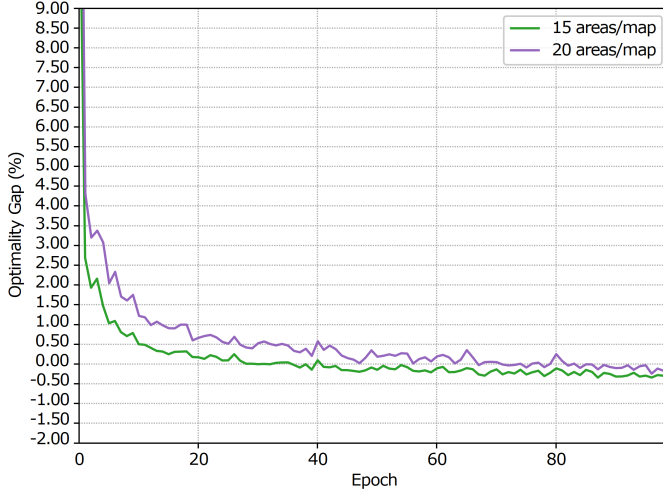


Fig. 5: Optimality gap for the network choosing the pattern.

normalization, as described in Section IV-A. To address that, the elements of E were scaled by 100 and rounded. Moreover, E was symmetrized using the method described in [37].

On the other hand, the same setup was applied in the RL environment, where the network was expected to learn the correct starting point, resulting in a 0% optimality gap. The results, shown in Fig. 5, indicate that the agent successfully learned to solve the TSP under this constraint. Toward the end of the training, the model even produced slightly better results, reflected as a negative optimality gap in Fig. 5. This slight improvement is due to the approximations described earlier, which had to be done to obtain a solution from Concorde. The distances in the edge weight matrix (i.e., the distances from the exit point to the starting point) are

$$a_{ij} = \begin{cases} \|p_{i_exit} - p_{j_start}\|_2, & \text{if } i \neq j \\ 0 & \text{otherwise.} \end{cases} \quad (13)$$

C. System Assessment

After combining all decoder parts to test the full system, we found that fixing starting and stopping points yielded results matching the ground truth. As shown in Fig. 6, the framework consistently achieved a negative optimality gap, with the gap increasing as the number of areas grew. This suggests that the total distance becomes more sensitive to starting and stopping points with more areas. Additionally, testing with a critic baseline network showed that a rollout baseline provided better results, as learning with a fixed baseline is more effective than learning with a moving target.

D. Scaling Capabilities

To evaluate the model's capabilities with varying numbers of areas, we increased the number of areas within the unit square space to 30, 40, and 50. It is important to note that the model was trained using samples with maximum 20 areas.

The results of 1000 randomly generated test cases are summarized in TABLE I. TRATSS outperformed Concorde

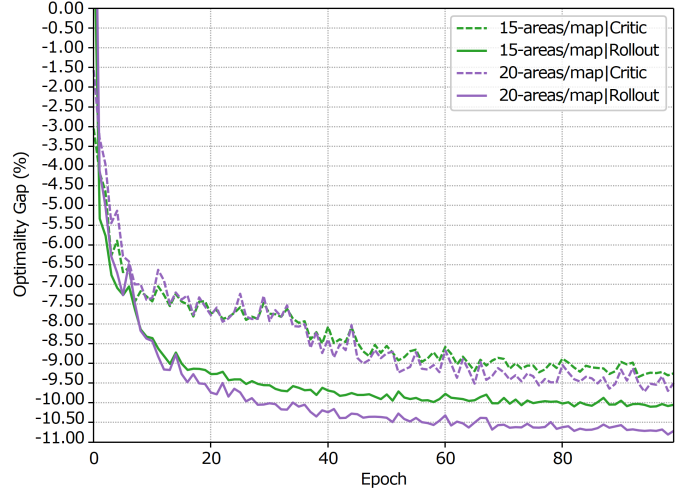


Fig. 6: Optimality gap for the whole TRATSS framework.

TABLE I: Costs for a unit squared area.

Number of Areas	Concorde		TRATSS	
	μ [m]	σ [m]	μ [m]	σ [m]
20	4.39	0.34	3.90	0.33
30	5.26	0.35	4.68	0.33
40	6.01	0.39	5.45	0.33
50	6.77	0.46	6.23	0.34

in all tested scenarios, achieving an average improvement of approximately 10%.

In addition to these results, we investigated the robustness of Concorde and the proposed method using boxplots, as shown in Fig. 7. The boxplots compare the performance, measured in terms of cost, of baseline models (denoted as C_{20} to C_{50}) and the proposed models (denoted as M_{20} to M_{50}) across different configurations.

Across all configurations, the proposed model (M -) achieved consistently lower mean costs compared to the corresponding baseline models (C -). For example, for 20 areas, the mean cost for M_{20} is 3.91, notably lower than 4.39 for C_{20} . This trend persists for 30 areas, where M_{30} achieves a mean cost of 4.68 compared to 5.26 for C_{30} .

At higher configurations, such as 50 areas, the proposed M_{50} model shows a mean cost of 6.23 compared to 6.77 for C_{50} . The consistent reduction in mean values across all configurations highlights the effectiveness of the proposed models in minimizing cost.

Additionally, the proposed M - exhibit lower standard deviations compared to the baseline models, indicating reduced variability and greater stability. For instance, M_{20} has a standard deviation of 0.33, slightly lower than 0.34 for C_{20} . This trend is more pronounced in higher configurations, such as 50 areas, where M_{50} has a standard deviation of 0.34 compared to 0.46 for C_{50} . Additionally, the proposed method showed a narrower inter-quartile range for all tested scenarios. These results combined suggest that the proposed method is more robust under varying conditions.

Overall, the results demonstrate the superiority of the

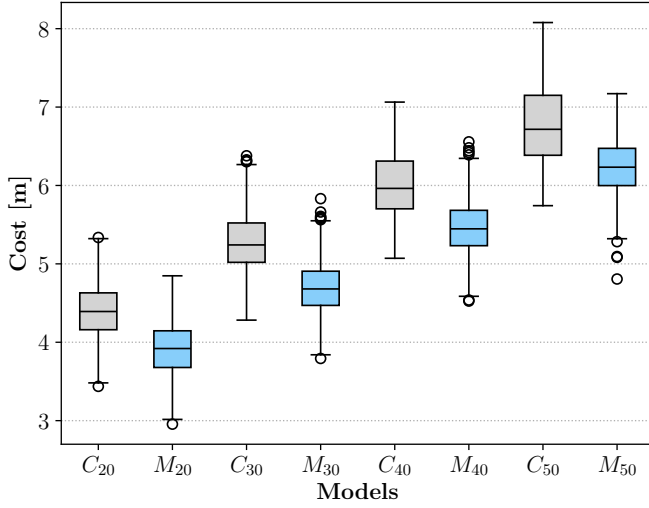


Fig. 7: Boxplots comparing the performance of Concorde and the proposed method with different numbers of areas.

proposed method over Concorde in both performance and robustness. The consistent reduction in mean cost and lower standard deviations across all configurations underline the potential of the proposed approach in outperforming traditional baseline methods.

The optimization achieved with the proposed method can lead to significant gains in real-world applications. For example, assuming an overall gain of 10%, an agent operating in a scenario such as search and rescue would travel fewer kilometers, potentially saving time and resources, both of which are critical and sensitive in such applications.

VII. CONCLUSION

This paper introduced TRATSS, a novel framework combining combinatorial optimization with transformer architecture for the implementation of a systems-level solution for single-agent time-extended task scheduling. The proposed method was tested extensively to understand its potential and capabilities in scaled problems. Overall, TRATSS demonstrated its effectiveness in task scheduling, outperforming heuristic combinatorial optimization tools like Concorde TSP solver. In addition, TRATSS showed strong generalization capabilities, offering fast and efficient solutions, making it suitable for real-world applications. Moreover, the high-level nature of the system makes it applicable to contexts where different types of agents are used. The system can be a very effective component for mission planning, especially in time-sensitive missions which involve complex planning problems, as TRATSS can provide fast high quality solutions.

REFERENCES

- [1] X. Chen, L. Cheng, C. Liu, Q. Liu, J. Liu, Y. Mao, and J. Murphy, "A woa-based optimization approach for task scheduling in cloud computing systems," *IEEE Systems Journal*, vol. 14, no. 3, pp. 3117–3128, 2020.
- [2] W. F. Mahmudy, A. W. Widodo, and A. H. Haikal, "Challenges and opportunities for applying meta-heuristic methods in vehicle routing problems: A review," *Engineering Proceedings*, vol. 63, no. 1, 2024. [Online]. Available: <https://www.mdpi.com/2673-4591/63/1/12>
- [3] E. Karpas and D. Magazzeni, "Automated planning for robotics," *Annual Review of Control, Robotics, and Autonomous Systems*, vol. 3, no. Volume 3, 2020, pp. 417–439, 2020. [Online]. Available: <https://www.annualreviews.org/content/journals/10.1146/annurev-control-082619-100135>
- [4] M. Rezvani, M. K. Akbari, and B. Javadi, "Resource allocation in cloud computing environments based on integer linear programming," *The Computer Journal*, vol. 58, no. 2, pp. 300–314, 2015.
- [5] K. E. Booth, G. Nejat, and J. C. Beck, "A constraint programming approach to multi-robot task allocation and scheduling in retirement homes," in *Principles and Practice of Constraint Programming: 22nd International Conference, CP 2016, Toulouse, France, September 5-9, 2016, Proceedings 22*. Springer, 2016, pp. 539–555.
- [6] W. F. Mahmudy, M. Z. Sarwani, A. Rahmi, A. W. Widodo, and U. Pasuruan, "Optimization of multi-stage distribution process using improved genetic algorithm," *Int J Intell Eng Syst*, vol. 14, no. 2, pp. 211–219, 2021.
- [7] J. Li, C. Huang, and Z. Shen, "Multi-objective vehicle routing problem with time windows based on improved simulated annealing algorithm," in *Second International Conference on Advanced Algorithms and Signal Image Processing (AASIP 2022)*, vol. 12475. SPIE, 2022, pp. 445–452.
- [8] I. Bello, H. Pham, Q. V. Le, M. Norouzi, and S. Bengio, "Neural combinatorial optimization with reinforcement learning," in *International Conference on Learning Representations*, ser. Workshop Poster Sessions, 2017.
- [9] T. Brown, B. Mann, N. Ryder, M. Subbiah, J. D. Kaplan, P. Dhariwal, A. Neelakantan, P. Shyam, G. Sastry, A. Askell *et al.*, "Language models are few-shot learners," *Advances in neural information processing systems*, vol. 33, pp. 1877–1901, 2020.
- [10] S. Bubeck, V. Chandrasekaran, R. Eldan, J. Gehrke, E. Horvitz, E. Kamar, P. Lee, Y. T. Lee, Y. Li, S. Lundberg *et al.*, "Sparks of artificial general intelligence: Early experiments with gpt-4," *arXiv preprint arXiv:2303.12712*, 2023.
- [11] A. Vaswani, N. Shazeer, N. Parmar, J. Uszkoreit, L. Jones, A. N. Gomez, L. Kaiser, and I. Polosukhin, "Attention is all you need," *Advances in neural information processing systems*, vol. 30, 2017.
- [12] Z. Niu, H. Liu, X. Lin, and J. Du, "Task scheduling with uav-assisted dispersed computing for disaster scenario," *IEEE Systems Journal*, vol. 16, no. 4, pp. 6429–6440, 2022.
- [13] B. Park, C. Kang, and J. Choi, "Cooperative multi-robot task allocation with reinforcement learning," *Applied Sciences*, vol. 12, no. 1, 2022. [Online]. Available: <https://www.mdpi.com/2076-3417/12/1/272>
- [14] K. Li, T. Liu, P. Ram Kumar, and X. Han, "A reinforcement learning-based hyper-heuristic for AGV task assignment and route planning in parts-to-picker warehouses," *Transportation Research Part E: Logistics and Transportation Review*, vol. 185, p. 103518, 2024. [Online]. Available: <https://www.sciencedirect.com/science/article/pii/S1366554524001091>
- [15] J. Wang, C. Liu, Y. Zhao, Z. Zhao, Y. Ma, M. Liu, and W. Shen, "Graph convolutional network aided inverse graph partitioning for resource allocation," *IEEE Transactions on Industrial Informatics*, vol. 20, no. 3, pp. 3082–3091, 2024.
- [16] C. K. Joshi, Q. Cappart, L.-M. Rousseau, and T. Laurent, "Learning the travelling salesperson problem requires rethinking generalization," *Constraints*, vol. 27, no. 1, pp. 70–98, 2022.
- [17] Q. Li, W. Lin, Z. Liu, and A. Prorok, "Message-aware graph attention networks for large-scale multi-robot path planning," *IEEE Robotics and Automation Letters*, vol. 6, no. 3, pp. 5533–5540, 2021.
- [18] J. Xu and Z. He, "A GNN-based mission planning approach coupled with environment for multiple unmanned ground vehicles," in *2023 6th International Conference on Software Engineering and Computer Science (CSECS)*, 2023, pp. 1–6.
- [19] J. Wang, J. Wang, and H. Che, "Task assignment for multivehicle systems based on collaborative neurodynamic optimization," *IEEE Transactions on Neural Networks and Learning Systems*, vol. 31, no. 4, pp. 1145–1154, 2020.
- [20] O. Rivlin, T. Hazan, and E. Karpas, "Generalized planning with deep reinforcement learning," *arXiv preprint arXiv:2005.02305*, 2020.
- [21] L. Antonyshyn, J. Silveira, S. Givigi, and J. Marshall, "Multiple mobile robot task and motion planning: A survey," *ACM Comput. Surv.*, vol. 55, no. 10, Feb. 2023. [Online]. Available: <https://doi.org/10.1145/3564696>
- [22] B. Wang, Z. Liu, Q. Li, and A. Prorok, "Mobile robot path planning in dynamic environments through globally guided reinforcement learning," *IEEE Robotics and Automation Letters*, vol. 5, no. 4, pp. 6932–6939, 2020.
- [23] Z. Chen, J. Alonso-Mora, X. Bai, D. D. Harabor, and P. J. Stuckey, "Integrated task assignment and path planning for capacitated multi-

agent pickup and delivery,” *IEEE Robotics and Automation Letters*, vol. 6, no. 3, pp. 5816–5823, 2021.

- [24] X. Bai, Y. Ye, B. Zhang, and S. S. Ge, “Efficient package delivery task assignment for truck and high capacity drone,” *IEEE Transactions on Intelligent Transportation Systems*, vol. 24, no. 11, pp. 13422–13435, 2023.
- [25] B. Yin, J. Li, and X. Wei, “Rational task assignment and path planning based on location and task characteristics in mobile crowdsensing,” *IEEE Transactions on Computational Social Systems*, vol. 9, no. 3, pp. 781–793, 2022.
- [26] J. Huang, J. Wan, B. Lv, Q. Ye, and Y. Chen, “Joint computation of flooding and resource allocation for edge-cloud collaboration in internet of vehicles via deep reinforcement learning,” *IEEE Systems Journal*, vol. 17, no. 2, pp. 2500–2511, 2023.
- [27] X. Huang, K. Yang, and J. Ling, “Large vehicle scheduling based on uncertainty weighting harmonic twin-critic network,” *IEEE Systems Journal*, 2023.
- [28] M. S. A. Hameed and A. Schwung, “Graph neural networks-based scheduler for production planning problems using reinforcement learning,” *Journal of Manufacturing Systems*, vol. 69, pp. 91–102, 2023. [Online]. Available: <https://www.sciencedirect.com/science/article/pii/S0278612523001097>
- [29] A. Salehipour, K. Sörensen, P. Goos, and O. Bräysy, “Efficient grasp+vnd and grasp+vns metaheuristics for the traveling repairman problem,” *4OR*, vol. 9, pp. 189–209, 06 2011.
- [30] M. Bruni, P. Beraldi, and S. Khodaparasti, “A hybrid reactive grasp heuristic for the risk-averse k-traveling repairman problem with profits,” *Computers & Operations Research*, vol. 115, p. 104854, 2020. [Online]. Available: <https://www.sciencedirect.com/science/article/pii/S0305054819302965>
- [31] X. Bresson and T. Laurent, “An experimental study of neural networks for variable graphs,” *ICLR Workshop*, 2018.
- [32] G. Brockman, V. Cheung, L. Pettersson, J. Schneider, J. Schulman, J. Tang, and W. Zaremba, “Openai gym,” *arXiv preprint arXiv:1606.01540*, 2016.
- [33] I. Zamora, N. G. Lopez, V. M. Vilches, and A. H. Cordero, “Extending the openai gym for robotics: a toolkit for reinforcement learning using ros and gazebo,” *arXiv preprint arXiv:1608.05742*, 2016.
- [34] N. G. Lopez, Y. L. E. Nuin, E. B. Moral, L. U. S. Juan, A. S. Rueda, V. M. Vilches, and R. Kojcev, “gym-gazebo2, a toolkit for reinforcement learning using ros 2 and gazebo,” *arXiv preprint arXiv:1903.06278*, 2019.
- [35] S. J. Mahajan, D. L. Applegate, W. J. Cook, and A. R. Bixby, “Concorde tsp solver,” <http://www.math.uwaterloo.ca/tsp/concorde>, [Online; accessed: Dec. 12, 2024].
- [36] W. Kool, H. Van Hoof, and M. Welling, “Attention, learn to solve routing problems!” *arXiv preprint arXiv:1803.08475*, 2018.
- [37] R. Jonker and T. Volgenant, “Transforming asymmetric into symmetric traveling salesman problems,” *Operations Research Letters*, vol. 2, no. 4, pp. 161–163, 1983. [Online]. Available: <https://www.sciencedirect.com/science/article/pii/0167637783900482>



Yazan Youssef (GSM’23) received an M.Sc. degree in Electrical Engineering from the American University of Sharjah (AUS), Sharjah, UAE. He is now a Ph.D. candidate in the Electrical and Computer Engineering department at Queen’s University, Kingston, ON, Canada. His research interests include planning in autonomous systems and robotics, automation, and machine learning.



Paulo Ricardo Marques de Araujo (M’24) received a Ph.D. in Electrical and Computer Engineering from Queen’s University, Kingston, ON, Canada, and is currently a Postdoctoral Researcher at the School of Computing. During his Ph.D., he researched localization systems for autonomous vehicles, focusing on the integration of multiple sensors, advanced filtering techniques, and deep learning. His broader research interests include autonomous systems, robotics, machine learning, and digital manufacturing.



Aboelmagd Noureldin (SM’08) Dr. Aboelmagd Noureldin is a Professor and Canada Research Chair (CRC) at the Department of Electrical and Computer Engineering, Royal Military College of Canada (RMC), with Cross-Appointment at both the School of Computing and the Department of Electrical and Computer Engineering, Queen’s University. He is also the founding director of the Navigation and Instrumentation (NavINST) research group at RMC, a unique world-class research facility in GNSS, wireless positioning, inertial navigation, remote sensing and multisensory fusion for navigation and guidance. Dr. Noureldin holds a Ph.D. in Electrical and Computer Engineering (2002) from The University of Calgary, Alberta, Canada. In addition, he has a B.Sc. in Electrical Engineering (1993) and an M.Sc. degree in Engineering Physics (1997), both from Cairo University, Egypt. Dr. Noureldin is a Senior member of the IEEE and a professional member of the Institute of Navigation (ION). He published two books, four book chapters, and over 350 papers in academic journals, conferences, and workshop proceedings, for which he received several awards. Dr. Noureldin’s research led to 13 patents and several technologies licensed to industry in position, location and navigation systems.



Sidney Givigi (SM’14) received a Ph.D. in Electrical and Computer Engineering from Carleton University, Ottawa, ON, Canada. He is now a Professor with the School of Computing of Queen’s University, Kingston, ON. Sidney’s research interests mainly focus on machine learning, autonomous systems, and robotics.